

# Individualized Treatment Effects with Censored Data via Fully Nonparametric Bayesian Accelerated Failure Time Models

Nicholas C. Henderson<sup>1</sup>, Thomas A. Louis<sup>2</sup>, Gary L. Rosner<sup>1,2</sup>, and Ravi Varadhan<sup>1,2</sup>

<sup>1</sup> Sidney Kimmel Comprehensive Cancer Center, Johns Hopkins University

<sup>2</sup> Department of Biostatistics, Bloomberg School of Public Health, Johns Hopkins University

## Abstract

Individuals often respond differently to identical treatments, and characterizing such variability in treatment response is an important aim in the practice of personalized medicine. In this article, we describe a non-parametric accelerated failure time model that can be used to analyze heterogeneous treatment effects (HTE) when patient outcomes are time-to-event. By utilizing Bayesian additive regression trees and a mean-constrained Dirichlet process mixture model, our approach offers a flexible model for the regression function while placing few restrictions on the baseline hazard. Our non-parametric method leads to natural estimates of individual treatment effect and has the flexibility to address many major goals of HTE assessment. Moreover, our method requires little user input in terms of tuning parameter selection or subgroup specification. We illustrate the merits of our proposed approach with a detailed analysis of two large clinical trials for the prevention and treatment of congestive heart failure using an angiotensin-converting enzyme inhibitor. The analysis revealed considerable evidence for the presence of HTE in both trials as demonstrated by substantial estimated variation in treatment effect and by high proportions of patients exhibiting strong evidence of having treatment effects which differ from the overall treatment effect.

*Keywords:* Dirichlet Process Mixture; Ensemble Methods; Heterogeneity of Treatment Effect; Interaction; Personalized Medicine; Subgroup Analysis.



# 1 Introduction

While the main focus of clinical trials is on evaluating the average effect of a particular treatment, assessing heterogeneity in treatment effect (HTE) across key patient sub-populations remains an important task in evaluating the results of clinical studies. Accurate evaluations of HTE that is attributable to variation in baseline patient characteristics offers many potential benefits in terms of informing patient decision-making and in appropriately targeting existing therapies. HTE assessment can encompass a wide range of goals: quantification of overall heterogeneity in treatment response, identification of important patient characteristics related to HTE, estimation of proportion who benefits from the treatment, identification of patient sub-populations deriving most benefit from treatment, detection of cross-over (qualitative) interactions, identifying the patients who are harmed by treatment, estimation of individualized treatment effects, optimal treatment allocation for individuals, and predicting treatment effect for a future patient.

Recently, there has been increasing methodology development in the arena of HTE assessment. However, each developed method has been targeted to address one specific goal of HTE analysis. For example, Xu et al. (2015), Foster et al. (2011) and Berger et al. (2014) developed a method to identify patient subgroups whose response to treatment differs substantially from the average treatment effect. Weisberg and Pontes (2015) and Lamont et al. (2016) discuss estimation of individualized treatment effects. Zhao et al. (2012) and Zhao et al. (2015) discuss construction of optimal individualized treatment rules through minimization of a weighted classification error. Shen and Cai (2016) focus on detection of biomarkers which are predictive of treatment effect heterogeneity. Thus, none of the existing methods is sufficiently flexible to address multiple goals of HTE analysis.

Our aim in this paper is to construct a unified methodology for analyzing and exploring HTE with a particular focus on cases where the responses are time-to-event. The methodology is readily extended to continuous and binary response data. The motivation for investigating such a framework is the recognition that most, if not all, of the above-stated goals of personalized medicine could be directly addressed if a sufficiently rich approximation to the true data generating model for patient outcomes were available. Bayesian nonparametric methods are well-suited to provide this more unified framework for HTE analysis because they place few a priori restrictions on the form of the data-generating



model and provide great adaptivity. Bayesian nonparametrics allow construction of flexible models for patient outcomes coupled with probability modeling of all unknown quantities which generates a full posterior distribution over the desired response surface. This allows researchers to directly address a wide range of inferential targets without the need to fit a series of separate models or to employ a series of different procedures. Our methodology has the flexibility to address all of the HTE goals previously highlighted. For example, the researchers could quantify overall HTE; identify most important patient characteristics pertaining to HTE; estimate the proportion benefiting from, or harmed by, the treatment; and predict treatment effect for a future patient.

Bayesian additive regression trees (BART) (Chipman et al. (2010)) provide a flexible means of modeling patient outcomes without the need for making specific parametric assumptions, specifying a functional form for a regression model, or for using pre-specified patient subgroups. Because it relies on an ensemble of regression trees, BART has the capability to automatically detect non-linearities and covariate interactions. As reported by Hill (2011) in the context of using BART for causal inference, BART has the advantage of exhibiting strong predictive performance in a variety of settings while requiring little user input in terms of selecting tuning parameters. While tree-based methods have been employed in the context of personalized medicine and subgroup identification by a variety of investigators including, for example, Su et al. (2009), Loh et al. (2015), Chen and Chen (2016), and Foster et al. (2011), BART offers several advantages for the analysis of HTE. In contrast to many other tree-based procedures that use a more algorithmic approach, BART is model-based and utilizes a full likelihood function and corresponding prior over the tree-related parameters. Because of this, BART automatically generates measures of posterior uncertainty; on the other hand, reporting uncertainty intervals is often quite challenging for other frequentist tree-based procedures. In addition, because inference with BART relies on posterior sampling, analysis of HTE on alternative treatment scales can be done directly by simply transforming the desired parameters in posterior sampling. Moreover, any quantity of interest for individualized decisions or HTE evaluation can be readily accommodated by the Bayesian framework. In this paper, we aim to utilize and incorporate these advantages of BART into our approach for analyzing HTE with censored data.

Extensions of the original BART procedure to handle time-to-event outcomes have been proposed and investigated by Bonato et al. (2011) and Sparapani et al. (2016). In



Bonato et al. (2011), the authors introduce several sum-of-trees models and examine their use in utilizing gene expression measurements for survival prediction. Among the survival models proposed by Bonato et al. (2011) is an accelerated failure time (AFT) model with a sum-of-trees regression function and a normally distributed residual term. Sparapani et al. (2016) introduce a non-parametric approach that employs BART to directly model the individual-specific probabilities of an event occurring at the observed event and censoring times. In contrast to this approach, we propose a non-parametric version of the AFT model which combines a sum-of-trees model with a Dirichlet process mixture model for the residual distribution. Such an approach has the advantage of providing great flexibility while generating interpretable measures of covariate-specific treatment effects thus facilitating the analysis of HTE.

Accelerated failure time (AFT) models (Louis (1981), Robins and Tsiatis (1992), or Wei (1992)) represent an alternative to Cox-proportional hazards models in the analysis of time-to-event data. AFT models have a number of features which make them appealing in the context of personalized medicine and investigating the comparative effectiveness of different treatments. Because they involve a regression with log-failure times as the response variable, AFT models provide a direct interpretation of the relationship between patient covariates and failure times. Moreover, treatment effects may be defined directly in terms of the underlying failure times. Bayesian semi-parametric approaches to the accelerated failure time model have been investigated by a number of authors including Johnson and Christensen (1988), Kuo and Mallick (1997), Hanson and Johnson (2002), and Hanson (2006). Kuo and Mallick (1997) assume a parametric model for the regression function and suggest either modeling the distribution of the residual term or of the exponential of the residual term via a Dirichlet process mixture model, while Hanson (2006) proposed modeling the residual distribution with a Dirichlet process mixture of Gamma densities. Our approach for modeling the residual distribution resembles that of Kuo and Mallick (1997). Similar to these approaches, we model the residual distribution as a location-mixture of Gaussian densities, and by utilizing constrained Dirichlet processes, we constrain the mean of the residual distribution to be zero, thereby clarifying the interpretation of the regression function.

This paper is organized as follows. In Section 2, we describe the general structure of our nonparametric, tree-based accelerated failure time model, discuss its use in estimating



individualized treatment effects, and describe our approach for posterior computation. Section 3 examines several key inferential targets in the analysis of heterogeneous treatment effects and how the nonparametric AFT model may be utilized to estimate these targets. In Section 4, we detail the results of several simulation studies that evaluate our procedure in terms of individualized treatment effect estimation, coverage, and optimal treatment assignment. In Section 5, we examine a clinical trial involving the use of an ACE inhibitor, and we demonstrate the use of our nonparametric AFT method to investigate heterogeneity of treatment effect in this study. We conclude in Section 6 with a few final remarks. The methods described in this paper are implemented in the R package **AFTrees**, which is available for download at <http://www.hteguru.com/software>.

## 2 The Model

### 2.1 Notation and Non-parametric AFT model

We assume that study participants have been randomized to one of two treatments which we denote by either  $A = 0$  or  $A = 1$ . We let  $\mathbf{x}$  denote a  $p \times 1$  vector of baseline covariates and let  $T$  denote the failure time. Given a censoring time  $C$ , we observe  $Y = \min\{T, C\}$  and a failure indicator  $\delta = \mathbf{1}\{T \leq C\}$ . The data consist of  $n$  independent measurements  $\{(Y_i, \delta_i, A_i, \mathbf{x}_i); i = 1, \dots, n\}$ . Although we assume randomized treatment assignment here, our approach may certainly be applied in observational settings. In such settings, however, one should ensure that appropriate unconfoundedness assumptions (e.g., Hill (2011)) are reasonable, so that the individualized treatment effects defined in (2) correspond to an expected difference in potential outcomes under the two treatments.

The conventional accelerated failure time (AFT) model assumes that log-failure times are linearly related to patient covariates. We consider here a non-parametric analogue of the AFT model in which the failure time  $T$  is related to the covariates and treatment assignment through

$$\log T = m(A, \mathbf{x}) + W, \tag{1}$$

and where the distribution of the residual term  $W$  is assumed to satisfy  $E(W) = 0$ . With the mean-zero constraint on the residual distribution, the regression function  $m(A, \mathbf{x})$  has a direct interpretation as the expected log-failure time given treatment assignment and



baseline covariates.

The AFT model (1) leads to a natural, directly interpretable definition of the individualized treatment effect (ITE), namely, the difference in expected log-failure in treatment  $A = 1$  versus  $A = 0$ . Specifically, we define the ITE  $\theta(\mathbf{x})$  for a patient with covariate vector  $\mathbf{x}$  as

$$\begin{aligned}\theta(\mathbf{x}) &= E\{\log(T)|A = 1, \mathbf{x}, m\} - E\{\log(T)|A = 0, \mathbf{x}, m\} \\ &= m(1, \mathbf{x}) - m(0, \mathbf{x}).\end{aligned}\tag{2}$$

The distribution of  $T$  in the accelerated failure time model (1) is characterized by both the regression function  $m$  and the distribution  $F_W$  of the residual term. In the following, we outline a model for the regression function that utilizes additive regression trees, and we describe a flexible nonparametric mixture model for the residual distribution  $F_W$ .

## 2.2 Overview of BART

Bayesian Additive Regression Trees (BART) is an ensemble method in which the regression function is represented as the sum of individual regression trees. The BART model for the regression function relies on a collection of  $J$  binary trees  $\{\mathcal{T}_1, \dots, \mathcal{T}_J\}$  and an associated set of terminal node values  $B_j = \{\mu_{j,1}, \dots, \mu_{j,n_j}\}$  for each binary tree  $\mathcal{T}_j$ . Each tree  $\mathcal{T}_j$  consists of a sequence of decision rules through which any covariate vector can be assigned to one terminal node of  $\mathcal{T}_j$  by following the decision rules prescribed at each of the interior nodes. In other words, each binary tree generates a partition of the predictor space in which each element  $\mathbf{u} = (A, \mathbf{x})$  of the predictor space belongs to exactly one of the  $n_j$  terminal nodes of  $\mathcal{T}_j$ . The decision rules at the interior nodes of  $\mathcal{T}_j$  are of the form  $\{u_k \leq c\}$  vs.  $\{u_k > c\}$ , where  $u_k$  denotes the  $k^{th}$  element of  $\mathbf{u}$ . A covariate  $\mathbf{u}$  that corresponds to the  $l^{th}$  terminal node of  $\mathcal{T}_j$  is assigned the value  $\mu_{j,l}$  and  $g(A, \mathbf{x}; \mathcal{T}_j, B_j)$  is used to denote the function that returns  $\mu_{j,l} \in B_j$  whenever  $(A, \mathbf{x})$  is assigned to the  $l^{th}$  terminal node of  $\mathcal{T}_j$ .

The regression function  $m$  is represented in BART as a sum of the individual tree contributions

$$m(A, \mathbf{x}) = \sum_{j=1}^J g(A, \mathbf{x}; \mathcal{T}_j, B_j).\tag{3}$$

Trees  $\mathcal{T}_j$  and node values  $B_j$  can be thought of as model parameters with priors on these pa-



rameters inducing a prior on the regression function  $m$  via (3). To complete the description of the prior on  $(\mathcal{T}_1, B_1), \dots, (\mathcal{T}_J, B_J)$ , one needs to specify the following: (i) the distribution on the choice of splitting variable at each internal node; (ii) the distribution of the splitting value  $c$  used at each internal node; (iii) the probability that a node at a given node-depth  $d$  splits, which is assumed to be equal to  $\alpha(1+d)^{-\beta}$ ; and (iv) the distribution of the terminal node values  $\mu_{j,l}$  which is assumed to be  $\mu_{j,l} \sim \text{Normal}\{0, (4k^2J)^{-1}\}$ . In order to ensure that the prior variance for  $\mu_{j,l}$  induces a prior on the regression function that assigns high probability to the observed range of the data, Chipman et al. (2010) center and scale the response so that the minimum and maximum values of the transformed response are  $-0.5$  and  $0.5$  respectively. The distributions used for (i) and (ii) are discussed in Chipman et al. (1998) and Chipman et al. (2010).

To denote the distribution on the regression function  $m$  induced by the prior distribution on  $\mathcal{T}_j, B_j$  with parameter values  $(\alpha, \beta, k)$  and  $J$  total trees, we use the notation

$$m \sim \text{BART}(\alpha, \beta, k, J).$$

### 2.3 Centered DP mixture prior

We model the density  $f_W$  of  $W$  as a location-mixture of Gaussian densities with common scale parameter  $\sigma$ . Letting  $G$  denote the distribution of the locations, we assume the density of  $W$  (conditional on  $G$  and  $\sigma$ ) can be expressed as

$$f_W(w|G, \sigma) = \frac{1}{\sigma} \int \phi\left(\frac{w - \tau}{\sigma}\right) dG(\tau), \quad (4)$$

where  $\phi(\cdot)$  is the standard normal density function. The Dirichlet process (DP) is a widely used choice for a nonparametric prior on an unknown probability distribution, and the resulting DP mixture model for the distribution of  $W$  provides a flexible prior for the residual density. Indeed, a DP mixture model similar to (4) was used by Kuo and Mallick (1997) as a prior for a smooth residual distribution in a semi-parametric accelerated failure time model.

Because of the zero-mean constraint on the residual distribution, the Dirichlet process



is not an appropriate choice for a prior on  $G$ . A direct approach proposed by Yang et al. (2010) addresses the problem of placing mean and variance constraints on an unknown probability measure by utilizing a parameter-expanded version of the Dirichlet process which the authors refer to as the centered Dirichlet process (CDP). As formulated by Yang et al. (2010), the CDP with mass parameter  $M$  and base measure  $G_0$  has the following stick-breaking representation

$$\begin{aligned}
G &= \sum_{h=1}^{\infty} \pi_h \delta_{\tau_h} \\
\pi_h &= V_h \prod_{l < h} (1 - V_l), \quad h = 1, \dots, \infty \\
\tau_h &= \tau_h^* - \mu_{G^*}, \quad h = 1, \dots, \infty \\
V_h &\sim \text{Beta}(1, M), \\
\tau_h^* &\sim G_0, \quad h = 1, \dots, \infty,
\end{aligned} \tag{5}$$

where  $\mu_{G^*} = \sum_{h=1}^{\infty} \pi_h \tau_h^*$  and where  $\delta_{\tau}$  denotes a distribution that only consists of a point mass at  $\tau$ . We denote that a random measure  $G$  follows a centered Dirichlet process with the notation  $G \sim \text{CDP}(M, G_0)$ . From the above representation of the CDP, it is clear that the mixture model (4) for  $W$  and the assumption that  $G \sim \text{CDP}(M, G_0)$  together imply the mean-zero constraint, since the expectation of  $W$  can then be expressed as

$$E(W|G, \sigma) = \sum_{h=1}^{\infty} \tau_h \pi_h = \sum_{h=1}^{\infty} \tau_h^* \pi_h - \mu_{G^*} \sum_{h=1}^{\infty} \pi_h,$$

which equals zero almost surely.

For the scale parameter of  $f_W$ , we assume that  $\sigma^2$  follows an inverse chi-square distribution,  $\sigma^2 \sim \kappa\nu/\chi_{\nu}^2$ , with the default degrees of freedom  $\nu$  set to  $\nu = 3$ . Instead of specifying a particular value for the mass parameter, we allow for learning about this parameter by assuming  $M \sim \text{Gamma}(\psi_1, \psi_2)$  where  $\psi_1$  and  $\psi_2$  refer to the shape and rate parameters of Gamma distribution respectively.

Our non-parametric model that combines the BART model for the regression function



and DP mixture model for the residual density can now be expressed hierarchically as

$$\begin{aligned}\log T_i &= m(A_i, \mathbf{x}_i) + W_i, \quad W_i | \tau_i, \sigma^2 \sim N(\tau_i, \sigma^2), \text{ for } i = 1, \dots, n \\ m &\sim \text{BART}(\alpha, \beta, k, J), \quad \tau_i | G \sim G, \quad G | M \sim \text{CDP}(M, G_0) \\ \sigma^2 &\sim \kappa \nu / \chi_\nu^2, \quad M \sim \text{Gamma}(\psi_1, \psi_2).\end{aligned}\tag{6}$$

In our implementation, the base measure  $G_0$  is assumed to be Gaussian with mean zero and variance  $\sigma_\tau^2$ . Choosing  $G_0$  to be conjugate to the Normal distribution simplifies posterior computation considerably, but other choices of  $G_0$  could be considered. For example, a t-distributed base measure could be implemented by introducing an additional latent scale parameter.

## 2.4 Prior Specification

*Prior for Trees and Terminal Node Parameters.* For the hyperparameters of the trees  $\mathcal{T}_1, \dots, \mathcal{T}_J$ , we defer to the defaults suggested in Chipman et al. (2010); namely,  $\alpha = 0.95$ ,  $\beta = 2$ , and  $J = 200$ . These default settings seem to work quite well in practice, and in Section 5 we investigate the impact of varying  $J$  through cross-validation estimates of prediction performance.

As discussed in Section 2.2, the original description of BART in Chipman et al. (2010) employs a transformation of the response variable and sets the hyperparameter  $k$  to  $k = 2$  so that the regression function is assigned substantial prior probability to the observed range of the response. Because our responses  $Y_i$  are right-censored, we propose an alternative approach to transforming the responses and to setting the prior variance of the terminal node parameters. Our suggested approach is to first fit a parametric AFT model that only has an intercept in the model and that assumes log-normal residuals. This produces estimates of the intercept  $\hat{\mu}_{AFT}$  and the residual scale  $\hat{\sigma}_{AFT}$  which allows us to define the transformed “centered” responses as  $y_i^{tr} = y_i \exp\{-\hat{\mu}_{AFT}\}$ . Turning to the prior variance of the terminal node parameters  $\mu_{j,l}$ , we assign the terminal node values  $\mu_{j,l}$  the prior distribution  $\mu_{j,l} \sim \text{Normal}\{0, \zeta^2/(4Jk^2)\}$ , where  $\zeta = 4\hat{\sigma}_{AFT}$ . This prior on  $\mu_{j,l}$  induces a  $\text{Normal}\{0, 4\hat{\sigma}_{AFT}^2/k^2\}$  prior on the regression function  $m(A, \mathbf{x})$  and hence assigns approximately 95% prior probability to the interval  $[-4k^{-1}\hat{\sigma}_{AFT}, 4k^{-1}\hat{\sigma}_{AFT}]$ . Thus, the default setting of  $k = 2$  assigns 95% prior probability to the interval  $[-2\hat{\sigma}_{AFT}, 2\hat{\sigma}_{AFT}]$ . Note that



assigning most of the prior probability to the interval  $[-2\hat{\sigma}_{AFT}, 2\hat{\sigma}_{AFT}]$  is sensible because this corresponds to the regression function for the “centered” responses  $y_i^{tr}$  rather than the original responses.

As described in Chipman et al. (1998) and Chipman et al. (2010), the prior on the splitting values  $c$  used at each internal node is uniform over the finite set of available splitting values for the chosen splitting variable. In implementations of BART, the number of possible available splitting values is typically truncated so that it cannot exceed a pre-specified maximum value. The default setting used in the **BayesTree** package (Chipman and McCulloch (2016)) has a maximum of 100 possible split points for each covariate, and the default is to assign a uniform prior over potential split points that are equally spaced over the range of the covariate. An alternative option offered in **BayesTree** is to, for each covariate, assign a uniform prior over the observed quantiles of the covariate rather than the uniform prior over the observed range of the covariate. Our default choice is to use the uniform prior over covariate quantiles for the split point prior rather than the uniform prior over equally spaced points. With this quantile-based prior, we found, in many simulations, improved performance in terms of coverage.

*Residual Distribution Prior.* Under the assumed prior for the mass parameter, we have  $E[M|\psi_1, \psi_2] = \psi_1/\psi_2$  and  $\text{Var}(M|\psi_1, \psi_2) = \psi_1/\psi_2^2$ . We set  $\psi_1 = 2$  and  $\psi_2 = 0.1$  so that the resulting prior on  $M$  is relatively diffuse with  $E[M|\psi_1, \psi_2] = 20$ ,  $\text{Var}[M|\psi_1, \psi_2] = 200$ , and a prior mode of 10.

When setting the defaults for the remaining hyperparameters  $\kappa$  and  $\sigma_\tau^2$ , we adopt a similar strategy to that used by Chipman et al. (2010) for BART when calibrating the prior for the residual variance. There, they rely on a preliminary, rough overestimate  $\hat{\sigma}^2$  of the residual variance parameter  $\sigma^2$  and define the prior for  $\sigma^2$  in such a way that there is  $1 - q$  prior probability that  $\sigma^2$  is greater than the rough estimate  $\hat{\sigma}^2$ . Here,  $q$  may be regarded as an additional hyperparameter with the value of  $q$  determining how conservative the prior of  $\sigma^2$  is relative to the initial estimate of the residual variance. Chipman et al. (2010) suggest using  $q = 0.90$  as the default whenever  $\nu$  is set to  $\nu = 3$ .

Similar to the approach described above, we begin with a rough over-estimate  $\hat{\sigma}_W^2$  of the variance of  $W$  to calibrate our choices of  $\kappa$  and  $\sigma_\tau^2$ . A direct way of generating the estimate  $\hat{\sigma}_W^2$  is to fit a parametric AFT model with log-normal residuals and use the resulting estimate of the residual variance, but other estimates could potentially be used.



To connect the estimate  $\hat{\sigma}_W^2$  with the hyperparameters  $\kappa$  and  $\sigma_\tau^2$  described in (6), it is helpful to first note that the conditional variance of the residual term can be expressed as

$$\text{Var}(W|G, \sigma) = \sigma^2 + \sigma_\tau^2 \sum_{h=1}^{\infty} \frac{\pi_h}{\sigma_\tau^2} (\tau_h^* - \mu_{G^*})^2. \quad (7)$$

Our aim then is to select  $\kappa$  and  $\sigma_\tau^2$  so that the induced prior on the variance of  $W$  assigns approximately  $1 - q$  probability to the event  $\{\text{Var}(W|G, \sigma) > \hat{\sigma}_W^2\}$ , where  $\hat{\sigma}_W^2$  is treated here as a fixed quantity. As an approximation to the distribution of (7), we use the approximation that  $\sum_{h=1}^{\infty} \frac{\pi_h}{\sigma_\tau^2} (\tau_h^* - \mu_{G^*})^2$  has a  $\text{Normal}\{1, 2/(M+1)\}$  distribution (see Yamato (1984) or Appendix A for further details about this approximation). Assuming further that  $\kappa = \sigma_\tau^2$ , we have that the variance of  $W$  is approximately distributed as  $\sigma_\tau^2[\nu/\chi_\nu^2 + N(1, \{2(M+1)\}^{-1})]$  where  $M \sim \text{Gamma}(\psi_1, \psi_2)$ , and with this approximation, we can directly find a value of  $\sigma_\tau^2 = \kappa$  such that  $P\{\text{Var}(W|G, \sigma) \leq \hat{\sigma}_W^2\} = q$ . In contrast to the  $q = 0.9$  setting suggested in Chipman et al. (2010), we set the default to  $q = 0.5$ .

## 2.5 Posterior Computation

The original Gibbs sampler proposed in Chipman et al. (2010) works by sequentially updating each tree while holding all other  $J - 1$  trees fixed. As a result, each iteration of the Gibbs sampler consists of  $2J + 1$  steps where the first  $2J$  steps involve updating either one of the trees  $T_j$  or terminal node parameters  $M_j$  and the last step involves updating the residual variance parameter. The Metropolis-Hastings algorithm used to update the individual trees is discussed in Chipman et al. (1998). Our strategy for posterior computation is a direct extension of the original Gibbs sampler, viz., after updating trees and terminal node parameters, we update the parameters related to the residual distribution. Censored values are handled through a data augmentation approach where unobserved survival times are imputed in each Gibbs iteration.

To sample from the posterior of the CDP, we adopt the blocked Gibbs sampling approach described in Ishwaran and James (2001). In this approach, the mixing distribution  $G$  is truncated so that it only has a finite number of components  $H$  which is done by assuming that,  $V_h \sim \text{Beta}(1, M)$  for  $h = 1, \dots, H - 1$  and  $V_H = 1$ . This modification of the stick-breaking weights ensures that  $\sum_{h=1}^H \pi_h = 1$ . One advantage of using the truncation approximation is that it makes posterior inferences regarding  $G$  straightfor-



ward. Additionally, when truncating the stick-breaking distribution, using the CDP prior as opposed to a DP prior does not present any additional challenges for posterior computation because the unconstrained parameters  $\tau_h^*, \mu_{G^*}$  in (5) may be updated as described in Ishwaran and James (2001) with the parameters of interest  $\tau_h$  then being updated through the simple transformation  $\tau_h = \tau_h^* - \mu_{G^*}$ . The upper bound on the number of components  $H$  should be chosen to be relatively large (as a default, we set  $H = 50$ ), and in the Gibbs sampler, the maximum index of the occupied clusters should be monitored. If a maximum index equal to  $H$  occurs frequently in posterior sampling,  $H$  should be increased.

In the description of the Gibbs sampler, we use  $z_i$  to denote a latent variable that represents a transformed, imputed survival time, and we let  $y_i^c$  denote the “complete-data” survival times for the transformed survival times. That is,  $y_i^{c,tr} = y_i^{tr}$  if  $\delta_i = 1$  and  $y_i^{c,tr} = z_i$  if  $\delta_i = 0$ . For posterior computation related to the Dirichlet process mixture, we let  $S_i$  denote the cluster to which the  $i^{th}$  observation has been assigned. An outline of the steps involved in one iteration of our Gibbs sampler is provided below.

1. Update trees  $\mathcal{T}_1, \dots, \mathcal{T}_J$  and node parameters  $B_1, \dots, B_J$  using the Bayesian backfitting approach of Chipman et al. (2010) with  $\log y_i^{c,tr} - \tau_{S_i}$  as the responses. Using the updated  $\mathcal{T}_1, \dots, \mathcal{T}_J$  and  $B_1, \dots, B_J$ , update  $m(A_i, \mathbf{x}_i)$ ,  $i = 1, \dots, n$ .
2. Update cluster labels  $S_1, \dots, S_n$  by sampling with probabilities

$$P(S_i = h) \propto \pi_h \phi\left(\frac{\log y_i^{c,tr} - m(A_i, \mathbf{x}_i) - \tau_h}{\sigma}\right),$$

and tabulate cluster membership counts  $n_h = \sum_i \mathbf{1}\{S_i = h\}$ .

3. Sample stick-breaking weights  $V_h$ ,  $h = 1, \dots, H - 1$  as  $V_h \sim \text{Beta}(\alpha_h, \beta_h)$  where  $\alpha_h = 1 + n_h$  and  $\beta_h = M + \sum_{k=h+1}^H n_k$ . Set  $V_H = 1$ . The updated mixture proportions are then determined by  $\pi_h = V_h \prod_{k < h} (1 - V_k)$ , for  $h = 1, \dots, H$ .
4. Sample unconstrained cluster locations  $\tau_h^*$

$$\tau_h^* \sim \text{Normal}\left(\frac{\sigma_\tau^2}{n_h \sigma_\tau^2 + \sigma^2} \sum_{i=1}^n \{\log y_i^{c,tr} - m(A_i, \mathbf{x}_i)\} \mathbf{1}\{S_i = h\}, \frac{\sigma_\tau^2 \sigma^2}{n_h \sigma_\tau^2 + \sigma^2}\right),$$

and update constrained cluster locations  $\tau_h = \tau_h^* - \mu_{G^*}$ , where  $\mu_{G^*} = \sum_{h=1}^H \pi_h \tau_h^*$ .



5. Update mass parameter  $M \sim \text{Gamma}(\psi_1 + H - 1, \psi_2 - \sum_{h=1}^{H-1} \log(1 - V_h))$  and scale parameter  $\sigma^2 \sim \text{Inverse-Gamma}(\frac{\nu+n}{2}, \frac{\hat{s}^2 + \kappa\nu}{2})$ , where  $\hat{s}^2$  is given by

$$\hat{s}^2 = \sum_{h=1}^H \sum_{i=1}^n \{\log(y_i^{c,tr}) - m(A_i, \mathbf{x}_i) - \tau_h\}^2 \mathbf{1}\{S_i = h\}.$$

6. For each  $i \in \{k : \delta_k = 0\}$ , update  $z_i$  by sampling

$$\log z_i \sim \text{Truncated-Normal}(m(A_i, \mathbf{x}_i) + \tau_{S_i}, \sigma^2; \log y_i^{tr}),$$

and set  $y_i^{c,tr} = z_i$ . Here,  $X \sim \text{Truncated-Normal}(\mu, \sigma^2; a)$  means that  $X$  is distributed as  $Z|Z > a$  where  $Z \sim \text{Normal}(\mu, \sigma^2)$ .

Because we use the transformed responses  $\log(y_i^{tr}) = \log(y_i) - \hat{\mu}_{AFT}$  in posterior computation, we add  $\hat{\mu}_{AFT}$  to the posterior draws of  $m(A, \mathbf{x})$  in the final output.

### 3 Posterior Inferences for the Analysis of Heterogeneous Treatment Effects

The nonparametric AFT model (6) generates a full posterior over the entire regression function  $m(A, \mathbf{x})$  and the residual distribution. As such, this model has the flexibility to address a variety of questions related to heterogeneity of treatment effect. In particular, overall variation in response to treatment, proportion of patients likely to benefit from treatment along with individual-specific treatment effects and survival curves may all be defined in terms of parameters from the nonparametric AFT model.

#### 3.1 Individualized Treatment Effects

As discussed in Section 2.1, a natural definition of the individual treatment effects in the context of an AFT model is the difference in expected log-survival  $\theta(\mathbf{x}) = m(1, \mathbf{x}) - m(0, \mathbf{x})$ . Draws from the posterior distribution of  $(m(A_1, \mathbf{x}_1), \dots, m(A_n, \mathbf{x}_n))$  allow one to compute fully nonparametric estimates  $\hat{\theta}(\mathbf{x}_i)$  of the treatment effects along with corresponding 95% credible intervals. As is natural with an AFT model, the treatment difference  $\theta(\mathbf{x})$  in (2) is examined on the scale of log-survival time, but other, more interpretable scales on which to



report treatment effects could be easily computed. For example, ratios in expected survival times  $\xi(\mathbf{x})$  defined by

$$\xi(\mathbf{x}) = E\{T|A = 1, \mathbf{x}, m\} / E\{T|A = 0, \mathbf{x}, m\} = \exp\{\theta(\mathbf{x})\}$$

could be estimated via posterior output. Likewise, one could estimate differences in expected failure time by using both posterior draws of  $\theta(\mathbf{x})$  and of the residual distribution. Posterior information regarding treatment effects may be used to stratify patients into different groups based on anticipated treatment benefit. Stratification could be done using the posterior mean, the posterior probability of treatment benefit, or some other relevant measure.

### 3.2 Assessing Evidence Heterogeneity of Treatment Effect

As a way of detecting the presence of HTE, we examine the posterior probabilities of differential treatment effect

$$D_i = P\{\theta(\mathbf{x}_i) \geq \bar{\theta} | \mathbf{y}, \boldsymbol{\delta}\}, \quad (8)$$

along with closely related quantity

$$D_i^* = \max\{1 - 2D_i, 2D_i - 1\}, \quad (9)$$

where, in (8),  $\bar{\theta} = n^{-1} \sum_{i=1}^n \theta(\mathbf{x}_i)$  is the conditional average treatment effect. Note that  $\bar{\theta}$  is a model parameter that represents the average value of the individual  $\theta(\mathbf{x}_i)$  and does not represent a posterior mean. The posterior probability  $D_i$  is a measure of the evidence that the ITE  $\theta(\mathbf{x}_i)$  is greater or equal to  $\bar{\theta}$ , and thus we should expect both high and low values of  $D_i$  in settings where substantial HTE is present. Note that  $D_i^*$  approaches 1 as the value of  $D_i$  approaches either 0 or 1, and  $D_i^* = 0$  whenever  $D_i = 1/2$ . For a given individual  $i$ , we consider there to be strong evidence of a differential treatment effect if  $D_i^* > 0.95$  (equivalently, if  $D_i \leq 0.025$  or  $D_i \geq 0.975$ ), and we define an individual as having mild evidence of a differential treatment effect provided that  $D_i^* > 0.8$  (equivalently, if  $D_i < 0.1$  or  $D_i > 0.9$ ). For cases with no HTE present, the proportion of patients exhibiting strong evidence of differential treatment effect should, ideally, be zero or quite close to zero. For this reason, the proportion of patients with  $D_i^* > 0.95$  can potentially be a useful summary



measure for detecting the presence of HTE. In this paper, we do not explore explicit choices of a threshold for this proportion, but we examine, through a simulation study in Section 4.2, the value of this proportion for scenarios for which no HTE is present and later compare these simulation results with the observed proportion of patients in the SOLVD trials who exhibit strong evidence of differential treatment effect. It is worth mentioning that the quantity  $D_i^*$  represents evidence that the treatment effect for patient  $i$  differs from the overall treatment effect, and by itself, is not a robust indicator of HTE across patients in the trial. Rather, the *proportion* of patients with high values of  $D_i^*$  is what we use as a means of assessing evidence for HTE.

It is worth noting that the presence or absence of HTE depends on the treatment effect scale, and  $D_i$  is designed for cases, such as the AFT model, where HTE is difference in expected log-failure time. For example, it is possible to have heterogeneity on the log-hazard ratio scale while having zero differences in the ITEs  $\theta(\mathbf{x}_i)$  across patients.

### 3.3 Characterizing Heterogeneity of Treatment Effect

Variability in treatment effect across patients in the study is a prime target of interest when evaluating the extent of heterogeneous treatment effects from the results of a clinical trial. Assessments of HTE can be used to evaluate consistency of response to treatment across patient sub-populations or to assess whether or not there are patient subgroups that appear to respond especially strongly to treatment. In more conventional subgroup analyses (e.g., Jones et al. (2011)), heterogeneity in treatment effect is frequently reported in terms of the posterior variation in treatment effect across patient subgroups. While the variance of treatment effect is a useful measure, especially in the context of subgroup analysis, we can provide a more detailed view of HTE by examining the full distribution of the individualized treatment effects defined by (2) where the distribution may be captured by the latent empirical distribution function  $H_n(t) = \frac{1}{n} \sum_{i=1}^n \mathbf{1}\{\theta(\mathbf{x}_i) \leq t\}$ . Such an approach to examining the “distribution” of a large collection of parameters has been explored in Shen and Louis (1998) and Louis and Shen (1999). The distribution function  $H_n(t)$  may be regarded as a model parameter that can directly estimated by

$$\hat{H}_n(t) = \frac{1}{n} \sum_{i=1}^n P\{\theta(\mathbf{x}_i) \leq t | \mathbf{y}, \boldsymbol{\delta}\}, \quad (10)$$



and credible bands for  $H_n(t)$  may be obtained from posterior samples. For improved visualization of the spread of treatment effects, it is often better to display a density function  $\hat{h}_n(t)$  associated with (10) which could be obtained through direct differentiation of (10). Alternatively, a smooth estimate can be found by computing the posterior mean of a kernel function  $K_\lambda$  with bandwidth  $\lambda$

$$\hat{h}_n(t) = \frac{1}{n} \sum_{i=1}^n E\left\{K_\lambda(t - \theta(\mathbf{x}_i)) \middle| \mathbf{y}, \boldsymbol{\delta}\right\}. \quad (11)$$

The posterior of  $H_n(t)$  provides a direct assessment of the variation in the underlying treatment effects, and as such, serves as a useful overall evaluation of HTE.

### 3.4 Proportion Who Benefits

Another quantity of interest related to HTE is the proportion of patients who benefit from treatment. Such a measure has a direct interpretation and is also a useful quantity for assessing the presence of cross-over or qualitative interactions, namely, cases where the effect of treatment has the opposite sign as the overall average treatment effect. That is, for situations where an overall treatment benefit has been determined, a low estimated proportion of patients benefiting may be an indication of the existence of cross-over interactions.

Using the treatment differences  $\theta(\mathbf{x})$ , the proportion who benefit may be defined as

$$Q = \frac{1}{n} \sum_{i=1}^n \mathbf{1}\{\theta(\mathbf{x}_i) > 0\}. \quad (12)$$

Alternatively, one could define the proportion benefiting relative to a clinically relevant threshold  $\varepsilon > 0$ , i.e.,  $Q_\varepsilon = n^{-1} \sum_{i=1}^n \mathbf{1}\{\theta(\mathbf{x}_i) > \varepsilon\}$ . The posterior mean of  $Q$  is an average over patients of the posterior probabilities of treatment benefit  $\hat{p}_i = P\{\theta(\mathbf{x}_i) > 0 | \mathbf{y}, \boldsymbol{\delta}\}$ . Posterior probabilities of treatment benefit can be used for treatment assignment ( $\hat{p}_i > 1/2$  vs.  $\hat{p}_i \leq 1/2$ ), or as an additional summary measure of HTE where one, for example, could tabulate the proportion very likely to benefit from treatment  $\hat{p}_i > 0.99$  or the proportion likely to benefit from treatment  $\hat{p}_i > 0.90$ .



### 3.5 Treatment Allocation

Individualized treatment recommendations may be directly obtained by combining a fit of the non-parametric AFT model with a procedure minimizing the posterior risk associated with a chosen loss function. For instance, when trying to minimize the proportion of treatment misclassifications, one would assign treatment based on whether or not the posterior probability of the event  $\{\theta(\mathbf{x}) > 0\}$  was greater than 0.5. Alternatively, one could optimize a weighted mis-classification loss where mis-classifications are weighted by the corresponding magnitude  $|\theta(\mathbf{x})|$  of the treatment effect, in which case the optimal treatment decision would depend on the posterior mean of  $\mathbf{1}\{\theta(\mathbf{x}) > 0\} \times |\theta(\mathbf{x})|$ . Though we do not explore the issue in this paper, such approaches to individualized treatment allocation could potentially be used, for example, in the development of adaptive randomization strategies for clinical trials.

### 3.6 Individual-level Survival Functions

In terms of the quantities of the non-parametric AFT model (6), individual-specific survival curves are defined by

$$P\{T > t|A, \mathbf{x}, m, G, \sigma\} = 1 - \int \Phi\left(\frac{\log t - m(A, \mathbf{x}) - \tau}{\sigma}\right) dG(\tau).$$

Using the truncated distribution  $G_H$  as an approximation in posterior computation, the survival curves are given by

$$P\{T > t|A, \mathbf{x}, m, G_H, \sigma\} = 1 - \sum_{h=1}^H \Phi\left(\frac{\log t - m(A, \mathbf{x}) - \tau_h}{\sigma}\right) \pi_h, \quad (13)$$

which may be directly estimated using posterior draws of the regression function and  $\tau_h, \pi_h$ .

### 3.7 Partial Dependence and Variable Importance

Partial dependence plots are a useful tool for visually assessing the dependence of an estimated function on a particular covariate or set of covariates. As described in Friedman (2001), such plots demonstrate the way an estimated function changes as a particular covariate varies while averaging over the remaining covariates.



For the purposes of examining the impact of a covariate on the treatment effects, we define the partial dependence function for the  $l^{th}$  covariate as

$$\rho_l(z) = \frac{1}{n} \sum_{i=1}^n \theta(z, \mathbf{x}_{i,-l}),$$

where  $(z, \mathbf{x}_{i,-l})$  denotes a vector where the  $l^{th}$  component of  $\mathbf{x}_i$  has been removed and replaced with the value  $z$ . Estimated partial dependence functions  $\hat{\rho}_l(z)$  with associated credible bands may be obtained directly from MCMC output.

## 4 Simulations

To evaluate the performance of the non-parametric, tree-based AFT method, we performed three simulation studies. For performance related to quantifying HTE, we recorded the following measures: root mean-squared error of the estimated individualized treatment effects, the proportion of patients allocated to the wrong treatment, and the average coverage of the confidence/credible intervals. For each simulation, the root mean-squared error (RMSE) is measured as  $\sqrt{n^{-1} \sum_{i=1}^n \{\hat{\theta}(\mathbf{x}_i) - \theta(\mathbf{x}_i)\}^2}$ , where  $\theta(\mathbf{x}_i)$  is as defined in Section 2.1, and  $\hat{\theta}(\mathbf{x}_i)$  is an estimate of the ITE. For treatment classification indicators  $R_1, \dots, R_n$  (i.e.,  $R_i = 1$  if patient  $i$  is classified as benefiting from treatment  $A = 1$  rather than  $A = 0$ ), the proportion mis-classified (MCprop) is calculated within each simulation replication as

$$\text{MCprop} = n^{-1} \sum_{i=1}^n \mathbf{1}\{\theta(\mathbf{x}_i) \leq 0\} R_i + n^{-1} \sum_{i=1}^n \mathbf{1}\{\theta(\mathbf{x}_i) > 0\} (1 - R_i).$$

Coverage proportions are measured as the average coverage over individuals, namely,  $n^{-1} \sum_{i=1}^n \mathbf{1}\{\hat{\theta}^L(\mathbf{x}_i) \leq \theta(\mathbf{x}_i) \leq \hat{\theta}^U(\mathbf{x}_i)\}$ , for interval estimates  $[\hat{\theta}^L(\mathbf{x}_i), \hat{\theta}^U(\mathbf{x}_i)]$ .

For the performance measures of RMSE and coverage proportions, we compared our tree-based non-parametric AFT model (NP-AFTree) with the semi-parametric AFT model (SP-AFTree) where the BART model is used for the regression function and the residual distribution is assumed to be Gaussian. In addition, we compared the NP-AFTree procedure with a parametric AFT model (Param-AFT) which assumes a linear regression with treatment-covariate interactions and log-normal residuals.

For both the NP-AFTree and SP-AFTree methods, 7,000 MCMC iterations were used



with the first 2,000 treated as burn-in steps. For both of these, the default parameters (i.e.,  $q = 0.5$ ,  $k = 2$ ,  $J = 200$ ) were used for each simulation scenario.

## 4.1 AFT simulations based on the SOLVD trials

In our first set of simulations, we use data from the SOLVD trials (The SOLVD Investigators (1991)) to guide the structure of the simulated data. Further details regarding the SOLVD trials are discussed in Section 5. To generate our simulated data, we first took two random subsets of sizes  $n = 200$  and  $n = 1,000$  from the SOLVD data. For each subset, we computed estimates  $\tilde{m}^{200}(A, \mathbf{x})$  and  $\tilde{m}^{1000}(A, \mathbf{x})$  respectively of the regression function for  $A \in \{0, 1\}$  using the non-parametric AFT Tree model. Simulated responses  $y_k$  were then generated as

$$\log y_k = A_{k(n)}\tilde{m}^n(0, \mathbf{x}_{k(n)}) + (1 - A_{k(n)})\tilde{m}^n(1, \mathbf{x}_{k(n)}) - 0.4 + W_k, \quad k = 1, \dots, n, \quad (14)$$

where the regression function was fixed across simulation replications and  $(A_{k(n)}, \mathbf{x}_{k(n)})$  corresponds to the  $k^{th}$  patient’s treatment assignment and covariate vector in the random subset with  $n$  patients. The constant  $-0.4$  in (14) was added so that there was a substantial fraction of simulated patients would have an underlying ITE  $\theta(\mathbf{x}) = \tilde{m}(1, \mathbf{x}) - \tilde{m}(0, \mathbf{x}) - 0.4$  less than zero. In particular, 44.1% of patients in the  $n = 1,000$  simulations had an underlying value of  $\theta(\mathbf{x})$  greater than zero while 88.5% had positive values of  $\theta(\mathbf{x})$ . For the distribution of  $W_k$ , we considered four different choices: a Gaussian distribution, a Gumbel distribution with mean zero, a “standardized” Gamma distribution with mean zero, and a mixture of three t-distributions with 3 degrees of freedom for each mixture component. The parameters of each of the four distributions were chosen so that the variances were approximately equal. The levels of censoring was varied across three levels: none, light censoring (approximately 15% of cases censored), and heavy censoring (45% of cases censored).

Mean-squared error, classification (MCprop), and coverage results are shown in Figure 1. More detailed results from this simulation study are displayed in the supplementary material. As may be inferred from Figure 1, the NP-AFTree method consistently performs better in terms of root mean-squared error and misclassification proportion than the SP-AFTree procedure. Moreover, while not apparent from the figure, the NP-AFTree approach



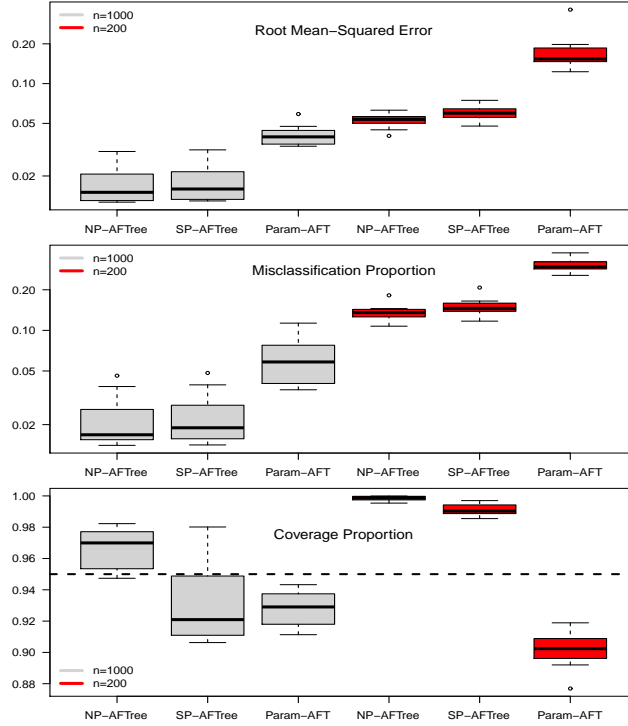


Figure 1: Simulations based on the SOLVD trial data. Results are based on 50 simulation replications. Root mean-squared error, Misclassification proportion, and empirical coverage are shown for each method. Performance measures are shown for the non-parametric tree-based AFT (NP-AFTree) method, the semi-parametric tree-based AFT (SP-AFTree), and the parametric, linear regression - based AFT (Param-AFT) approach. Four different choices of the residual distribution were chosen: a Gaussian distribution, a Gumbel distribution with mean zero, a “standardized” Gamma distribution with mean zero, and a mixture of three t-distributions with 3 degrees of freedom for each mixture component.

performs just as well as SP-AFTree, even when the true residual distribution is Gaussian (see the supplementary material). For each residual distribution, the advantage of NP-AFTree over SP-AFTree is more pronounced for the smaller sample sizes settings  $n = 200$ , with closer performance for the  $n = 1,000$  cases. While root mean-squared error and misclassification seem to be comparable between NP-AFTree and SP-AFTree for the  $n = 1,000$  settings, the coverage for NP-AFTree is consistently closer to the desired 95% level and is greater than 95% for nearly all settings. When  $n = 200$ , coverage often differs substantially from 95%, but in these cases, BART is quite conservative in the sense that coverage is typically much greater than 95%.

## 4.2 Several “Null” Simulations

We considered data generated from several “null” cases where the simulation scenarios were designed so that no HTE was present. For these simulations, we consider data generated



from four AFT models and data generated from a Cox proportional hazards model. In these “null” simulations, we are primarily interested in the degree to which the NP-AFTree procedure “detects” spurious HTE in situations where no HTE is present in the underlying data generating model. The AFT models used for the simulations assumed a linear regression function with no treatment-covariate interactions

$$\log y_k = \beta_0 + \beta_1 A_i + \sum_k \beta_k x_{ik} + W_i, \quad (15)$$

and the hazard functions for the Cox model simulations similarly took the form

$$h(t|\mathbf{x}) = h_0(t) \exp(\beta_0 + \beta_1 A_i + \sum_k \beta_k x_{ik}). \quad (16)$$

Although there may be a degree of heterogeneity in  $\theta(\mathbf{x})$  for the Cox proportional hazards model (16), it is still worthwhile to investigate the behavior of  $D_i$  when there is no HTE when treatment effects are defined in terms of hazard ratios.

The parameters in (15) were first estimated from the SOLVD data using a parametric AFT model with log-normal residuals. Here, we estimated the parameters in (15) separately using the same fixed subsets of size  $n = 1,000$  and  $n = 200$  used in Section 4.1. The parameters were fixed across simulation replications. For the AFT models, we considered the same four choices of the residual term distribution as in Section 4.1. The parameters for the hazard functions in (16) were found by fitting a Cox proportional hazards model to the same two subsets of size  $n = 200$  and  $n = 1,000$  from the SOVLD trials data, and these parameters were fixed across simulation replications. The cumulative baseline hazard function used to generate the Cox proportional hazards simulations was found by using Breslow’s estimator. In these simulations, we ran the NP-AFTree procedure with 2,000 MCMC iterations with the first 1,000 treated as burn-in steps.

For each null simulation scenario, we computed the posterior probabilities of differential treatment effect  $D_i$  (see equations (8) and 9) and tabulated the percentage of patients with either strong evidence of differential treatment effect (i.e.,  $D_i^* > 0.95$ ) or mild evidence (i.e.,  $D_i^* > 0.8$ ). Table 1 shows, for each null simulation scenario, the average proportion of individuals exhibiting strong evidence of a differential treatment effect and the average proportion of individuals exhibiting mild evidence of a differential treatment effect. As



displayed in Table 1, the average percentage of individuals showing strong evidence of differential treatment effect is less than 0.22% for all simulation settings. Moreover, the percentages of cases with mild evidence of differential treatment effect was fairly modest. The average percentage of patients with mild evidence was less than 3.9% for all except one simulation scenario, and most of the simulation scenarios had, on average, less than 3% of patients exhibiting mild evidence of differential treatment effect. Null simulations with  $n = 200$  tended to have much fewer cases of strong or mild evidence than those simulations with  $n = 1,000$ . The results presented in Table 1 suggest that the NP-AFTree procedure rarely reports any patients as having strong evidence of differential treatment effects for situations where HTE is absent.

Table 1: Simulation for settings without any HTE present. Results are based on 100 simulation replications. Average *percentage* of patients exhibiting strong evidence (SE) of differential treatment effect (i.e.  $D_i \geq 0.95$  or  $D_i \leq 0.05$ ) and average *percentage* of patients exhibiting mild evidence (ME) of differential treatment effect (i.e.,  $D_i \geq 0.8$  or  $D_i \leq 0.2$ ). Results are shown for AFT models with the same four residual distributions used in the simulations from Section 4.1 and for a Cox-proportional hazards model with no treatment-covariate interactions. Censoring levels were varied according to: none, light censoring (approximately 25% of cases censored), and heavy censoring (approximately 45% of cases censored).

n	Censoring	Normal		Gumbel		Std-Gamma		T-mixture		Cox-PH	
		SE	ME	SE	ME	SE	ME	SE	ME	SE	ME
200	none	0.000	0.095	0.000	0.040	0.000	0.070	0.000	0.060	0.000	0.140
200	light	0.000	0.095	0.000	0.000	0.075	0.350	0.000	0.380	0.000	0.015
200	heavy	0.000	0.020	0.000	0.000	0.000	0.000	0.000	0.055	0.000	0.290
1000	none	0.000	0.803	0.073	2.066	0.092	1.483	0.161	3.087	0.176	3.824
1000	light	0.061	1.989	0.015	0.967	0.213	2.674	0.066	3.176	0.111	3.405
1000	heavy	0.002	1.253	0.000	0.484	0.030	1.176	0.123	2.953	0.135	2.688

### 4.3 Friedman’s Randomly Generated Functions

In these simulations, we further evaluate the performance of the NP-AFTree using randomly generated nonlinear regression functions. To generate these random functions, we use a similar approach to that used in Friedman (2001) to assess the performance of gradient boosted regression trees. This approach allows us to test our approach on a wide range of difficult nonlinear regression functions that have higher-order interactions. For these simulations, we generated random regression functions  $m(A, \mathbf{x})$  via

$$m(A, \mathbf{x}_i) = F_0(\mathbf{x}_i) + A_i\theta(\mathbf{x}_i),$$



where the functions  $F_0(\mathbf{x})$  and  $\theta(\mathbf{x})$  are defined as

$$F_0(\mathbf{x}_i) = \sum_{l=1}^{10} a_{1l} g_{1l}(\mathbf{z}_{1l}) \quad \text{and} \quad \theta(\mathbf{x}_i) = \sum_{l=1}^5 a_{2l} g_{2l}(\mathbf{z}_{2l}). \quad (17)$$

The coefficients in (17) are generated as  $a_{1l} \sim \text{Uniform}(-1, 1)$  and  $a_{2l} \sim \text{Uniform}(-0.2, 0.3)$ . The vector  $\mathbf{z}_{jl}^i$  is a subset of  $\mathbf{x}_i$  of length  $n_{jl}$  where the randomly selected indices used to construct the subset of  $\mathbf{x}_i$  are the same for each  $i$ . The subset sizes are generated as  $n_{jl} = \min(\lfloor r_l + 1.5 \rfloor, 10)$  where  $r_{jl} \sim \text{Exponential}(1/2)$ .

$$g_{jl}(\mathbf{z}_{jl}) = \exp \left\{ -\frac{1}{2}(\mathbf{z}_{jl} - \boldsymbol{\mu}_{jl})^T \mathbf{V}_{jl}(\mathbf{z}_{jl} - \boldsymbol{\mu}_{jl}) \right\}.$$

The elements  $\mu_{jlk}$  of the vector  $\boldsymbol{\mu}_{jl}$  are generated as  $\mu_{jlk} \sim \text{Normal}(0, 1)$ , and the random matrix  $\mathbf{V}_{jl}$  is generated as  $\mathbf{V}_{jl} = \mathbf{U}_{jl} \mathbf{D}_{jl} \mathbf{U}_{jl}^T$ , where  $\mathbf{D}_{jl} = \text{diag}\{d_{jl,1}, \dots, d_{jl,n_{jl}}\}$  with  $\sqrt{d_{jl,k}} \sim \text{Uniform}(0.1, 2)$  and where  $\mathbf{U}_{jl}$  is a random orthogonal matrix. We generated the covariate vectors  $\mathbf{x}_i = (x_{i,1}, \dots, x_{i,20})^T$  of length 20 independently with  $x_{i,k} \sim \text{Normal}(0, 1)$ . Treatment assignments  $A_i$  were generated randomly with  $P(A_i = 1) = 1/2$ . These simulation settings imply that  $\theta(\mathbf{x})$  is positive for roughly 87% of individuals. The parameters of the residual distributions were chosen so that the variances of each distribution were approximately equal.

Figure 2 shows simulation results for NP-AFTree, SP-AFTree, and the parametric AFT model. In this figure, we observe that root-mean squared error is broadly the same for the NP-AFTree and SP-AFTree methods with each of the tree methods exhibiting much better performance than Param-AFT. This similarity in RMSE of SP-AFTree and NP-AFTree seems attributable to the difficulty of estimating these regression functions which seems to overwhelm most of the advantages of more flexible modeling of the residual distribution. Compared to SP-AFTree, NP-AFTree shows modestly better classification performance, particularly for settings that have non-Gaussian residual distributions and for settings with the larger ( $n = 1,000$ ) sample size. However, as in the simulations of Section 4.1, there seems to be no advantage here of either NP-AFTree, SP-AFTree, or Param-AFT over the naive treatment allocation approach when the sample size is  $n = 200$ . These results suggest that fairly large sample sizes may be needed for there to be any advantage over the naive approach which simply allocates individuals to the treatment having the more



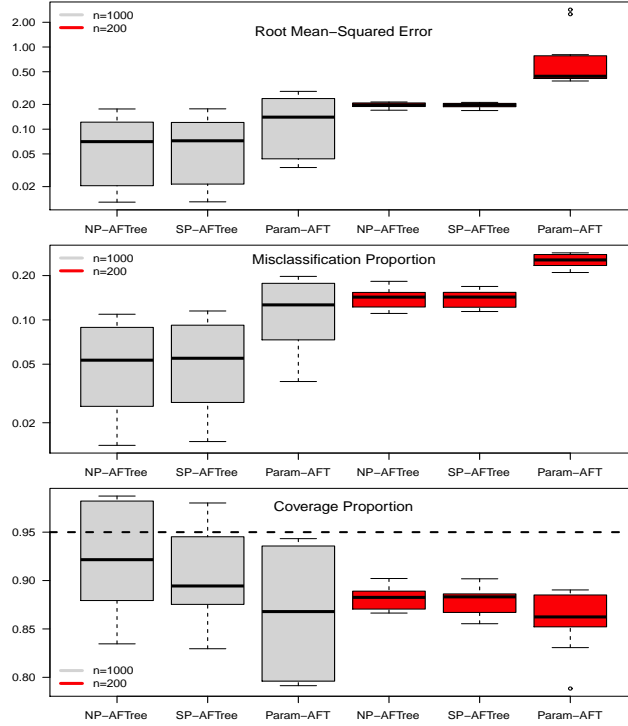


Figure 2: Simulations for AFT models with randomly generated regression functions. Results are based on 50 simulation replications. Root mean-squared error, misclassification proportion, and empirical coverage are shown for each method. Performance measures are shown for the non-parametric tree-based AFT (NP-AFTree) method, the semi-parametric tree-based AFT (SP-AFTree), and the parametric, linear regression - based AFT (Param-AFT) approach. Four different choices of the residual distribution were chosen: a Gaussian distribution, a Gumbel distribution with mean zero, a “standardized” Gamma distribution with mean zero, and a mixture of three t-distributions with 3 degrees of freedom for each mixture component.

beneficial overall treatment effect. For NP-AFTree the average coverage is consistently a few percentage points below the desired 95% level suggesting that modest under-coverage can occur in certain settings.

## 5 HTE in the SOLVD Trials

The Studies of Left Ventricular Dysfunction (SOLVD) were devised to investigate the efficacy of the angiotensin-converting enzyme (ACE) inhibitor enalapril in a target population with low left-ventricular ejection fractions. The SOLVD treatment trial (SOLVD-T) enrolled patients determined to have a history of overt congestive heart failure, and the SOLVD prevention trial (SOLVD-P) enrolled patients without overt congestive heart failure. In total, 2,569 patients were enrolled in the treatment trial while 4,228 patients were enrolled in the prevention trial. The survival endpoint that we examine in our analysis is



time until death or hospitalization where time is reported in days from enrollment.

In our analysis of the SOLVD-T and SOLVD-P trials, we included 18 patient covariates common to both trials, in addition to using treatment and study indicators as covariates. Of these 18 covariates, 8 were continuous covariates, 8 were binary covariates, one covariate was categorical with three levels, and one was categorical with four levels. In our analysis, we dropped those patients who had one or more missing covariate values, which resulted in 548 patients being dropped from the total of 6,797 enrolled in either trial.

## 5.1 Cross-Validation across Hyperparameter Settings

When fitting the NP-AFT model with the SOLVD data, we considered several settings for the hyperparameters, and for each setting of the hyperparameters, we computed cross-validation scores to evaluate performance in terms of predicting patient outcomes and in terms of characterizing HTE. For evaluating predictions of patient outcomes, we utilize, as in Tian et al. (2014) and Tian et al. (2007), a direct measure of absolute prediction error. In particular, for the  $k^{th}$  test set  $\mathcal{D}_k$ , we compute the following cross-validation score

$$CV_k^{abs} = \frac{1}{n_k} \sum_{i \in \mathcal{D}_k} \frac{\delta_i}{\hat{V}(Y_i|A_i, \mathbf{x}_i)} \left| \log Y_i - \hat{m}_{-\mathcal{D}_k}(A_i, \mathbf{x}_i) \right|, \quad (18)$$

where  $n_k$  is the number of patients in  $\mathcal{D}_k$  and  $\hat{m}_{-\mathcal{D}_k}(A, \mathbf{x})$  is the regression function estimated from the  $k^{th}$  training set. The weights used in (18)  $\hat{V}(Y_i|A_i, \mathbf{x}_i)$  are estimates of the censoring probability  $V(t|A, \mathbf{x}) = P(C > t|A, \mathbf{x})$ . The total K-fold cross-validation error is computed as  $K^{-1} \sum_{k=1}^K CV_k^{abs}$ .

Figure 3 shows results from applying cross-validation to the SOLVD trials with 36 different settings of the hyperparameters. The censoring probabilities  $\hat{V}(Y_i|A, \mathbf{x}_i)$  used as weights in (18) were estimated using a Cox model. The 36 hyperparameter settings were generated by varying the hyperparameter  $q$  which determines the parameters of the base distribution  $G_0$ , the hyperparameter  $k$  that determines the prior variance of the node values, and the number of trees  $J$ . We varied  $q$  across the four levels,  $q = 0.25, 0.5, 0.90, 0.99$ ;  $k$  across the three levels,  $k = 1, 2, 3$ ; and the number of trees  $J$  across the three levels,  $J = 50, 200, 400$ . Ten-fold cross-validation was used for each setting of the hyperparameters. As shown in Figure 3, the hyperparameter  $q$  appears to play the most important role in driving the differences in cross-validation performance while larger values of the shrinkage



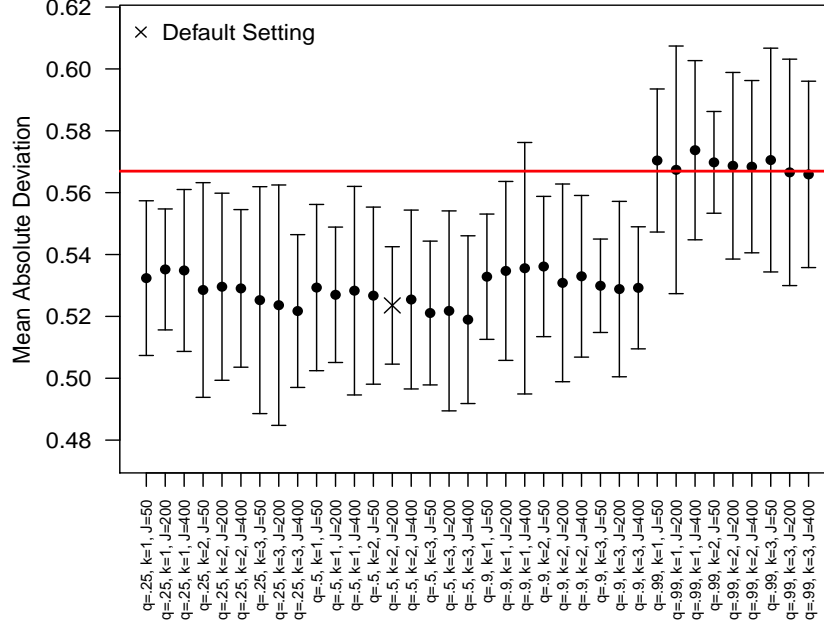


Figure 3: Ten-fold cross-validation for the SOLVD-T and SOLVD-P trials using the mean absolute deviation estimate defined in (18). Twenty seven settings of the hyperparameters are considered. The cross-validation score for the default setting of the hyperparameters is marked with an  $\times$ . The horizontal red line denotes the ten-fold cross-validation score of a parametric AFT model with log-normal errors where a linear regression model with treatment-covariate interactions was assumed.

parameter  $k$  seem to have a modest beneficial effect in the  $q = 0.25$  and  $q = 0.5$  settings. The settings with the very conservative choice of  $q = 0.99$  exhibit poor performance giving similar cross-validation scores as a parametric AFT model with an assumed linear model for the regression function. The setting with the best cross-validation score was  $q = 0.5, k = 3, J = 400$ . This cross-validation score, however, was not notably different than many of the settings with either  $q = 0.25$  and  $q = 0.5$ . For this reason, we continued to use the default setting of  $q = 0.5, k = 2$ , and  $J = 200$  in our analysis of the SOLVD trials.

## 5.2 Individualized Treatment Effect Estimates and Evidence for HTE

Figure 4 shows point estimates of the ITEs  $\theta(\mathbf{x})$  for patients in both the SOLVD-T and SOLVD-P trials. While the plot in Figure 4 indicates a clear, overall benefit from the treatment, the variation in the ITEs suggests substantial heterogeneity in response to treatment.

Examining the posterior probabilities of differential treatment effect offers further ev-



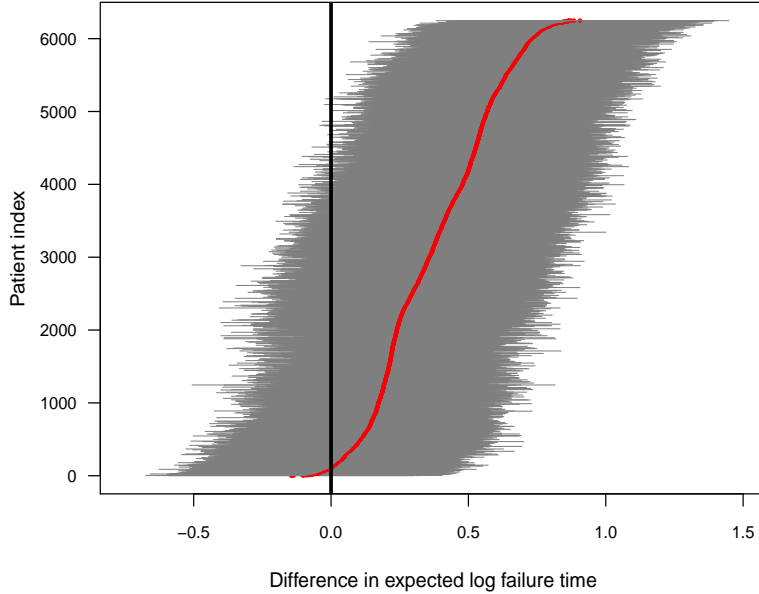


Figure 4: Posterior means of  $\theta(\mathbf{x})$  (red points) with corresponding 95% credible intervals for patients in the SOLVD-T and SOLVD-P trials.

idence for the presence of meaningful HTE in the SOLVD trials. Table 2 shows that, in the SOLVD-T trial, approximately 19% of patients had strong evidence of a differential treatment effect (i.e.  $D_i^* > 0.95$ ), and approximately 42% of patients had mild evidence of a differential treatment effect (i.e.,  $D_i^* > 0.80$ ). In the SOLVD-P trial approximately 7% of patients had strong evidence of a differential treatment effect while approximately 32% had mild evidence. Comparison of these percentages with the results from the simulations of Section 4.2 suggests the presence of HTE. In the null simulation scenarios of Section 4.2, the proportion of cases with strong evidence of differential treatment was very close to zero. Thus, the large proportion of patients with strong evidence for differential treatment effect is an indication of the presence of HTE in the SOLVD trials that deserves further exploration.

### 5.3 Characterizing Variation in Treatment Effect

Figure 5 displays a histogram of the posterior means of the treatment ratios  $\xi(\mathbf{x}) = E(T|A = 1, \mathbf{x}, m)/E(T|A = 0, \mathbf{x}, m)$ , for each patient in the SOLVD-T and SOLVD-P trials. In contrast to the ITE scale used in Figure 4, defining the ITEs in terms of the ratios of expected failure times may provide a more interpretable scale by which to describe HTE. As may be inferred from the histogram in Figure 5, nearly all patients have a



positive estimated treatment effect with 98.9% having an estimated value of  $\xi(\mathbf{x}_i)$  greater than one. Of those in the SOLVD-T trial, all the patients had  $E\{\xi(\mathbf{x}_i)|\mathbf{y}, \boldsymbol{\delta}\} > 1$ , and 98.2% of patients in the SOLVD-P trial had  $E\{\xi(\mathbf{x}_i)|\mathbf{y}, \boldsymbol{\delta}\} > 1$ .

Figure 5 also reports the smoothed estimate  $\hat{h}_n(t)$  of the distribution of the treatment effects separately for the two trials. These smoothed posterior estimates of the treatment effect distribution were computed as described in equation (11) where posterior samples of  $\xi(\mathbf{x}_i)$  were used in place of  $\theta(\mathbf{x}_i)$ . Note that the  $\hat{h}_n(t)$  shown in Figure 5 are estimates of the distribution of the underlying treatment effects and do not represent the posterior distribution of the overall treatment effects within each trial. As expected, the variation in treatment effect suggested by the plots of  $\hat{h}_n(t)$  in Figure 5 is greater than the variation exhibited by the posterior means of  $\xi(\mathbf{x}_i)$ . The estimates  $\hat{h}_n(t)$  provide informative characterizations of the distribution of treatment effects in each trial especially for visualizing the variability in treatment effects in each trial. The posterior median of the standard deviation of treatment effect  $\sqrt{\sum_i \{\xi(\mathbf{x}_i) - \bar{\xi}\}^2}$  was 0.45 for the SOLVD-T and 0.34 for the SOLVD-P trial.

## 5.4 Proportion Benefiting

We can use (12) to estimate the proportion of patients benefiting in each trial. The estimated proportions of patients (i.e., the posterior mean of  $Q$  in (12)) benefiting were 95.6% and 89.1% in the SOLVD-T and SOLVD-P trials respectively. These proportions are approximately equal to the area under the curve of  $\hat{h}_n(t)$  for  $t \geq 1$  in Figure 5.

Table 2 shows a tabulation of patients according to evidence of treatment benefit. In both trials, all patients have at least a 0.25 posterior probability of treatment benefit (i.e.  $P\{\xi(\mathbf{x}_i) > 1|\mathbf{y}, \boldsymbol{\delta}\} > 0.25$ ). In the treatment trial, 76% percent of patients exhibit a posterior probability of benefit greater than 0.95, and the percentage for the prevention trial is 44%.

## 5.5 Individual-level Survival Functions

Figure 6 shows estimated survival curves for randomly selected patients from the SOLVD treatment trial. Averages of these individual-level survival curves are computed for each treatment arm and compared with the corresponding Kaplan-Meier estimates of survival. It is apparent from Figure 6 that considerable heterogeneity in patient risk is present.



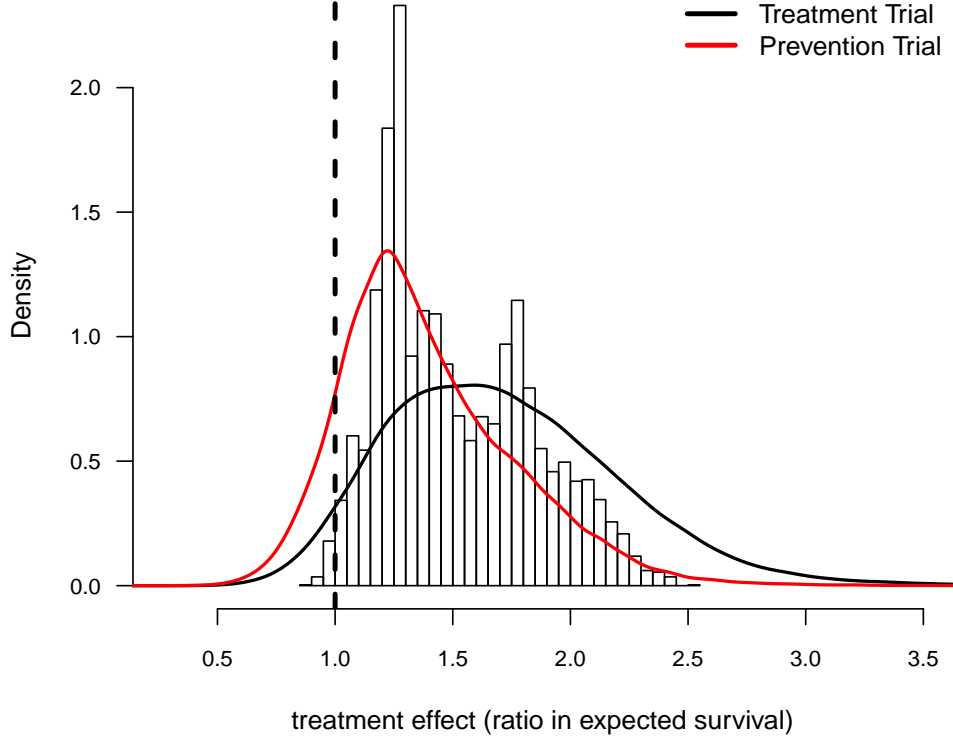


Figure 5: Histogram of point estimates (i.e., posterior means) of the treatment effects  $\xi(\mathbf{x}) = e^{\theta(\mathbf{x})}$  and smooth posterior estimates  $\hat{h}_n(t)$  of the treatment effect distribution. The histogram is constructed using all point estimates from both the SOLVD treatment and prevention trials. Smooth estimates,  $\hat{h}_n(t)$ , of the distribution of treatment effects were computed as described in equation for the two trials separately. The kernel bandwidth  $\lambda$  for each trial was chosen using the rule  $\lambda = [0.9 \times \min(\hat{\sigma}_\xi, I\hat{Q}R_\xi)]/[1.34 \times n_t^{1/5}]$ , where  $\hat{\sigma}_\xi$  and  $I\hat{Q}R_\xi$  are posterior means of the standard deviation and inter-quartile range of  $\xi(\mathbf{x}_i)$  respectively and where  $n_t$  is the trial-specific sample size.



	SOLVD Treatment Trial	SOLVD Prevention Trial
$P\{\xi(\mathbf{x}_i) > 1   \mathbf{y}, \boldsymbol{\delta}\} \in (0.99, 1]$	51.38	20.47
$P\{\xi(\mathbf{x}_i) > 1   \mathbf{y}, \boldsymbol{\delta}\} \in (0.95, 0.99]$	24.69	23.71
$P\{\xi(\mathbf{x}_i) > 1   \mathbf{y}, \boldsymbol{\delta}\} \in (0.75, 0.95]$	20.08	41.98
$P\{\xi(\mathbf{x}_i) > 1   \mathbf{y}, \boldsymbol{\delta}\} \in (0.25, 0.75]$	3.85	13.84
$P\{\xi(\mathbf{x}_i) > 1   \mathbf{y}, \boldsymbol{\delta}\} \in [0, 0.25]$	0.00	0.00
$D_i^* > 0.95$	19.36	7.30
$D_i^* > 0.80$	41.93	31.58

Table 2: Tabulation of posterior probabilities of treatment benefit and posterior probabilities of differential treatment effect  $D_i = P\{\xi(\mathbf{x}_i) \geq \xi | \mathbf{y}, \boldsymbol{\delta}\}$ . For each trial, the empirical percentage of patients whose estimated posterior probability of treatment benefit lies within each of the intervals  $(0.99, 1]$ ,  $(0.95, 0.99]$ ,  $(0.75, 0.95]$ ,  $(0.25, 0.75]$ , and  $[0, 0.25]$  is reported. In addition, the percentages of patients in each trial that exhibit “strong” (i.e.,  $D_i^* > .95$ ) and “mild” (i.e.,  $D_i^* > 0.80$ ) evidence of differential treatment effect are shown.

Indeed, in the control arm, 20% percent of patients had an estimated median survival time less than 500 days, 54% had between 500 and 1500 days, and 26% had an estimated median survival time of more than 1500 days.

## 5.6 Exploring Important Variables for HTE

To explore the patient attributes important in driving differences in treatment effect, we use a direct approach similar to the “Virtual Twins” method used by Foster et al. (2011) in the context of subgroup identification. In Foster et al. (2011), the authors suggest a two-stage procedure where one first estimates treatment difference for each individual and then, using these estimated differences as a new response variable, one estimates a regression model in order to identify a region of the covariate space where there is an enhanced treatment effect. Similarly, to examine important HTE variables, we first fit the full non-parametric AFT model to generate posterior means  $\hat{\theta}(\mathbf{x}_i)$  of the individualized treatment effect for each patient. Then, we estimate a regression using the previously estimated  $\hat{\theta}(\mathbf{x})$  as the response variable and the patient covariates (except for treatment assignment) as the predictors. Because the treatment difference  $\theta(\mathbf{x})$  should only depend on covariates that are predictive of HTE, using the unobserved  $\theta(\mathbf{x}_i)$  as the responses in a regression with the patient covariates as predictors represents a direct and efficient approach to exploring variables involved in driving treatment effect heterogeneity.

To investigate the important HTE variables in the SOLVD trials using the virtual twins approach, we fit a linear regression using weighted least squares with  $\hat{\theta}(\mathbf{x}_i)$  as the responses



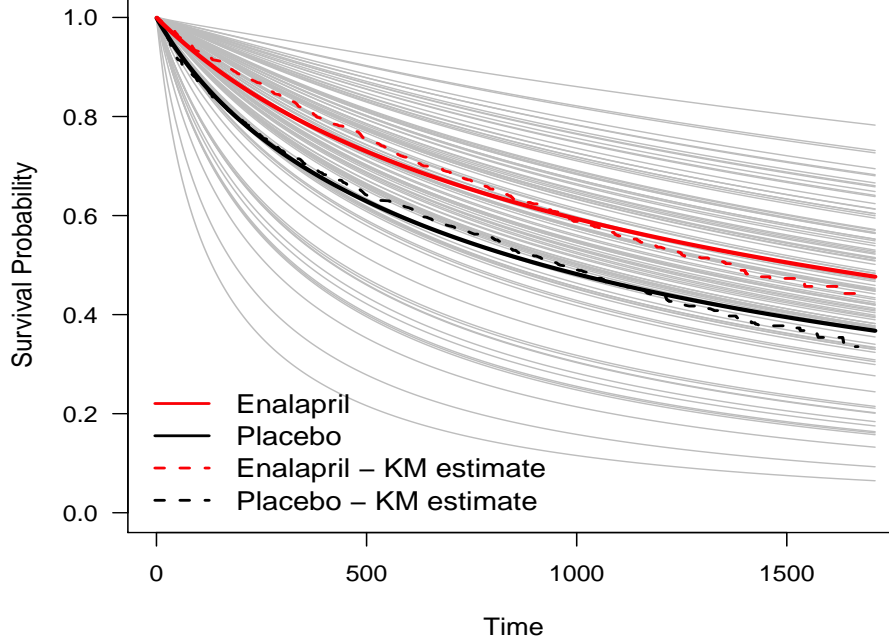


Figure 6: Estimates of individual-specific survival curves for selected patients from the SOLVD treatment trial. For each patient, the posterior mean of the survival functions  $P\{T > t|A, \mathbf{x}, m, G_H, \sigma\}$  as defined in (13) are plotted. The solid black and red survival curves are the average by treatment group of these estimated individual-specific curves. The dashed survival curves are the Kaplan-Meier estimates for each treatment group.

and where the residual variances were assumed proportional to the posterior variances of  $\theta(\mathbf{x}_i)$ . In this weighted regression, all covariates were normalized to have zero mean and unit variance. The patient covariates with the five largest estimated coefficients in absolute value were as follows: baseline ejection fraction, history of myocardial infarction, baseline creatinine levels, gender, and diabetic status. Figure 7 displays partial dependence plots for ejection fraction and creatinine along with the posterior distribution of the average treatment effect in the male/female groups and the subgroups defined by history of myocardial infarction. The partial dependence plots clearly demonstrate an enhanced treatment effect for those patients with lower baseline ejection fraction. The strongest change in treatment effect occurs in the ranges 0.20 – 0.30. The comparisons according to gender shown in Figure 7 show greater treatment benefit in men vs. women for both SOLVD trials.



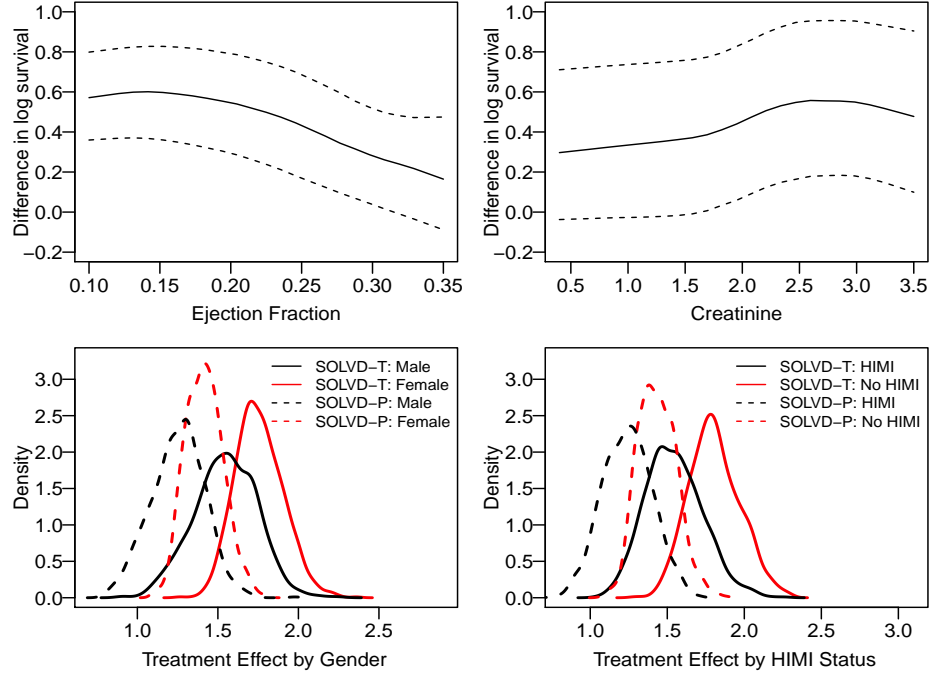


Figure 7: Smoothed partial dependence plots for ejection fraction and creatinine levels, and posterior distributions of treatment effect for men vs. women and for those with a history of myorcardial infarction vs. those with no history of myocardial infarction (HIMI vs. No HIMI).

## 6 Discussion

In this paper, we have described a flexible, tree-based approach to examining heterogeneity of treatment effect with survival endpoints. This method produces estimates of individualized treatment effects with corresponding credible intervals for AFT models with an arbitrary regression function and residual distribution. Moreover, we have demonstrated how this framework provides a useful framework for addressing a variety of other HTE-related questions. When using the default hyperparameter settings, the method only requires the user to input the survival outcomes, treatment assignments, and patient covariates. As shown in several simulation studies, the default settings exhibit strong predictive performance and good coverage properties. Though quite flexible, our non-parametric AFT model does entail some assumptions regarding the manner in which the patient covariates modify the baseline hazard. Hence, it would be worth further investigating the robustness of the nonparametric AFT method to other forms of model misspecification such as cases where neither an AFT or a Cox proportional hazards assumption holds or cases where the residual distribution depends on the patient covariates.



In addition to describing a novel non-parametric AFT model, we examined a number of measures for reporting HTE including the distribution of individualized treatment effects, the proportion of patients benefiting from treatment, and the posterior probabilities of differential treatment effect. Each have potential uses in allowing for more refined interpretations of clinical trial results. The argument has been made by some (e.g., Kent and Hayward (2007)) that the positive results of some clinical trials are driven substantially by the outcomes of high-risk patients. In such cases, the posterior distribution of the ITEs along with the estimated proportion benefiting may help in clarifying the degree to which lower risk patients are expected to benefit from the proposed treatment. In Section 4.2, we explored the use of posterior probabilities of differential treatment effect as a means of detecting the presence of HTE. Such measures show potential for evaluating the consistency of treatment and for assessing whether or not further investigations into HTE are warranted.

As described in this paper, the BART-based nonparametric AFT model only works when no missing values of the patient covariates occur. Though not explored in this paper, tree-based methods have the potential to provide intuitive, automatic approaches for handling missing data. In the “Missing in Attributes” approach discussed by Tiwala et al. (2008) and by Kapelner and Bleich (2015) for BART, the splitting rules are directly constructed to account for possible missingness. Such an approach could potentially be incorporated into the BART framework and allow one to handle missing covariates without needing to specify a method for imputation.

In the AFT model discussed in Sections 2.1 and 2.3, the distribution of the residual term is assumed to be the same for all values of the covariates. Greater flexibility may be gained by relaxing this assumption by considering an additional “heteroskedastic” AFT model which allows the residual distribution to change with the covariates. Although we do not fully explore the use of a heteroskedastic model in this work, one approach for modifying the nonparametric AFT model would be to allow the scale parameter of the residual density to depend on the patient covariates while having the mixing distribution remain independent of these covariates. One direct way of allowing the scale parameter to vary with the covariates would be to use a parametric log-linear model as described in the approach of Bleich and Kapelner (2014).

We note that our approach models the regression function  $m(A, \mathbf{x})$  for all values of  $A$



and  $\mathbf{x}$  in order to compute treatment effect contrasts  $m(1, \mathbf{x}) - m(0, \mathbf{x})$  and as such, requires modeling of both the “main effects” and the treatment-covariate interactions. This general approach to analyzing HTE - referred to as “global outcome modeling” by Lipkovich et al. (2016) - may be contrasted with other approaches that only seek to directly model the treatment effects without any consideration of the main effects. Modified outcome methods such as those described in Tian et al. (2014) and Weisberg and Pontes (2015) analyze modified response variables whose expectations have the desired treatment effects, and this approach allows one to directly estimate treatment-covariate interaction effects without having to model the main effects. Adopting an approach similar to this would be straightforward with our accelerated failure time model. One would only need to create modified responses by multiplying the observed log-failure times with an appropriate function of treatment assignment. These new responses would now exhibit different form of censoring, but this could easily be incorporated into our data augmentation procedure used in posterior sampling.



## A Approximate Distribution of the Residual Variance

As discussed in Section 2.4 of the main paper, the variance of the residual term may be expressed as

$$\text{Var}(W|G, \sigma) = \sigma^2 + \sigma_\tau^2 \sum_{h=1}^{\infty} \frac{\pi_h}{\sigma_\tau^2} (\tau_h^* - \mu_{G^*})^2 \quad (19)$$

When assuming (as we do) that  $\sigma_\tau^2 = \kappa$ , this becomes

$$\text{Var}(W|G, \sigma) = \sigma_\tau^2 \left[ \sigma^2 / \kappa + \sum_{h=1}^{\infty} \frac{\pi_h}{\sigma_\tau^2} (\tau_h^* - \mu_{G^*})^2 \right] \quad (20)$$

Because we assume that  $G \sim CDP(M, G_0)$  with  $G_0$  as a  $\text{Normal}(0, \sigma_\tau^2)$  distribution, the term  $[(\tau_h^* - \mu_{G^*})^2] / \sigma_\tau^2$  has a standard normal distribution.

In Section 2.4 of the main paper, it is stated that the prior distribution of  $\text{Var}(W|G, \sigma)$  is approximated with the following distribution

$$\sigma_\tau^2 [\nu / \chi_\nu^2 + \text{Normal}(1, \{2(M+1)\}^{-1})]. \quad (21)$$

The above approximation relies on the fact that  $\sum_{h=1}^{\infty} \frac{\pi_h}{\sigma_\tau^2} (\tau_h^* - \mu_{G^*})^2$  has an approximate  $\text{Normal}(0, \{2(M+1)\}^{-1})$  distribution in the sense described by Yamato (1984). A histogram of simulated values of  $\sum_{h=1}^{\infty} \frac{\pi_h}{\sigma_\tau^2} (\tau_h^* - \mu_{G^*})^2$  along with a plot of the approximating  $\text{Normal}(0, \{2(M+1)\}^{-1})$  density is shown in Figure 8. In this figure, histograms are shown for the cases of  $M = 25$  and  $M = 50$ .

In Figure 9, we display a quantile-quantile plot of simulated values from the distribution of  $\text{Var}(W|G, \sigma)$  vs. the approximate theoretical quantiles obtained from the approximate prior distribution stated in (21).



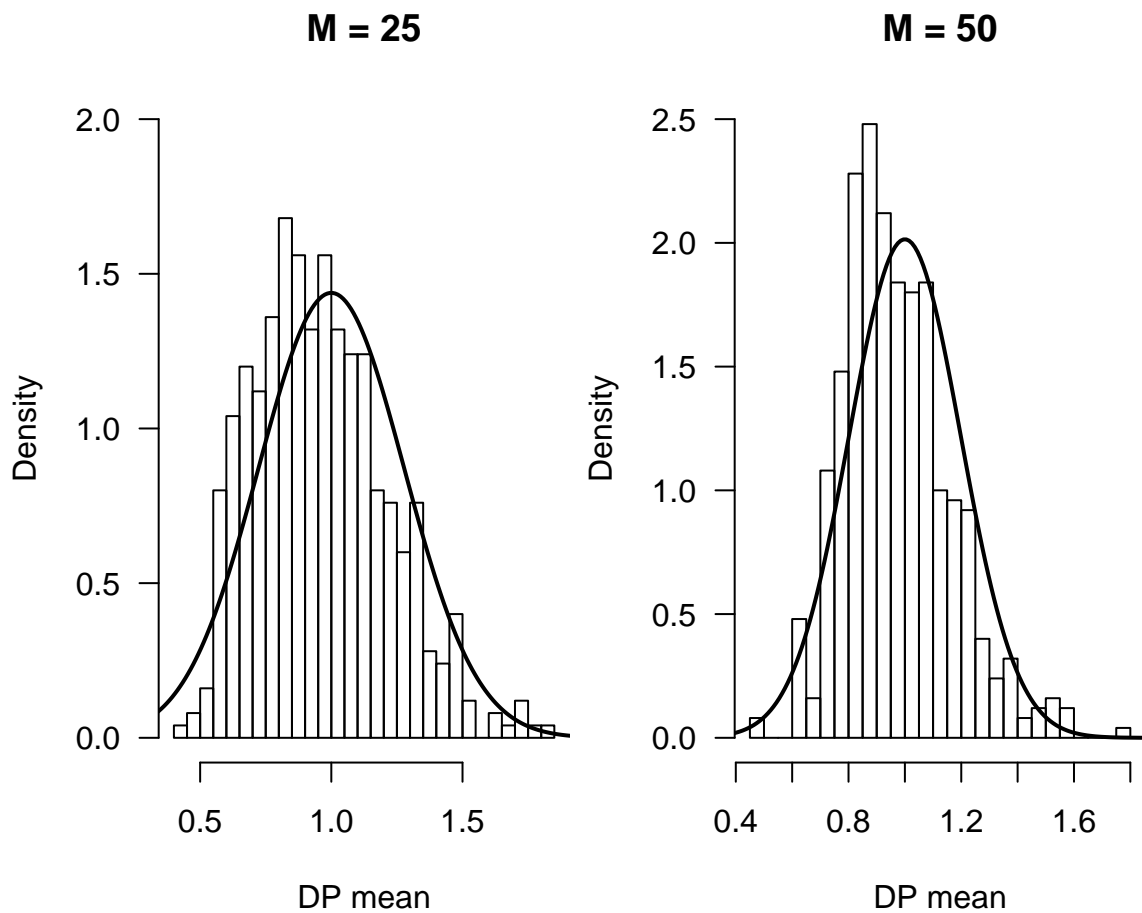


Figure 8: Histogram of simulated values of  $\sum_{h=1}^{\infty} \frac{\pi_h}{\sigma_{\tau}^2} (\tau_h^* - \mu_{G^*})^2$  along with the approximating  $\text{Normal}\{1, 2/(M+1)\}$  density. Simulations were performed with  $M = 25$  and  $M = 50$  for the mass parameter. In each case, 500 simulated values of  $a$  were drawn.



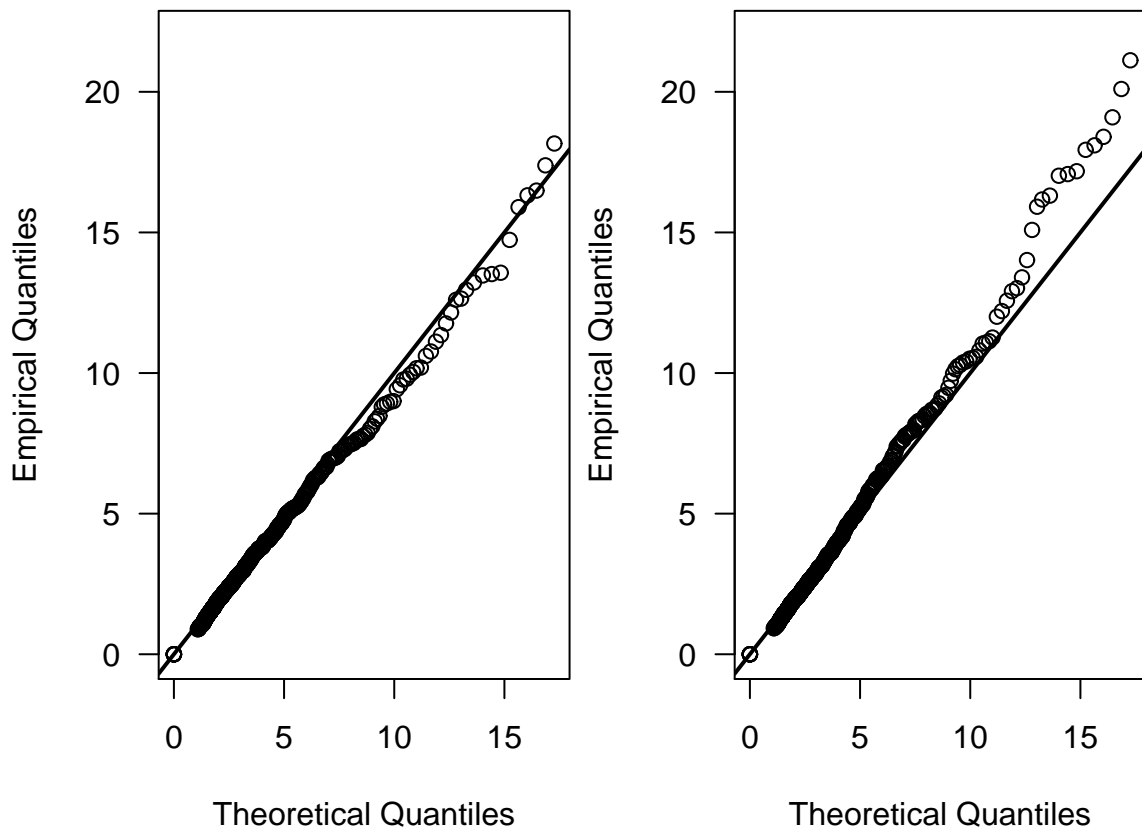


Figure 9: Quantile-Quantile plot with simulated values of  $\text{Var}(W|G, \sigma)$  (using equation).



## References

- Berger, J. O., X. Wang, and L. Shen (2014). A Bayesian approach to subgroup identification. *Journal of Biopharmaceutical Statistics* 24, 110–129.
- Bleich, J. and A. Kapelner (2014, February). Bayesian Additive Regression Trees With Parametric Models of Heteroskedasticity. *ArXiv e-prints*.
- Bonato, V., V. Baladandayuthapani, B. M. Broom, E. P. Sulman, K. D. Aldape, and K.-A. Do (2011). Bayesian ensemble methods for survival prediction in gene expression data. *Bioinformatics* 27(3), 359–367.
- Chen, Y.-C. and J. J. Chen (2016). Ensemble survival trees for identifying subpopulations in personalized medicine. *Biometrical Journal* 58(5), 1151–1163.
- Chipman, H. and R. McCulloch (2016). *BayesTree: Bayesian Additive Regression Trees*. R package version 0.3-1.4.
- Chipman, H. A., E. I. George, and R. E. McCulloch (1998). Bayesian CART model search (with discussion and a rejoinder by the authors). *Journal of the American Statistical Association* 93(443), 935–960.
- Chipman, H. A., E. I. George, and R. E. McCulloch (2010). BART: Bayesian additive regression trees. *The Annals of Applied Statistics* 4(1), 266–298.
- Foster, J. C., J. M. G. Taylor, and S. J. Ruberg (2011). Subgroup identification from randomized clinical trial data. *Statistics in Medicine* 30, 2867–2880.
- Friedman, J. (2001). Greedy function approximation: A gradient boosting machine. *The Annals of Statistics* 29(5), 1189–1232.
- Hanson, T. and W. O. Johnson (2002). Modeling regression error with a mixture of Polya trees. *Journal of the American Statistical Association* 97, 1020–1033.
- Hanson, T. E. (2006). Modeling censored lifetime data using a mixture of gammas baseline. *Bayesian Analysis* 1, 575–594.



- Hill, J. L. (2011). Bayesian nonparametric modeling for causal inference. *Journal of Computational and Graphical Statistics* 20(1), 217–240.
- Ishwaran, H. and L. F. James (2001). Gibbs sampling methods for stick-breaking priors. *Journal of the American Statistical Association* 96(453), 161–173.
- Johnson, W. and R. Christensen (1988). Modeling accelerated failure time with a Dirichlet process. *Biometrika* 75, 693–704.
- Jones, H., D. Ohlssen, B. Neuenschwander, A. Racine, and M. Branson (2011). Bayesian models for subgroup analysis in clinical trials. *Clinical Trials* 8, 129 – 143.
- Kapelner, A. and J. Bleich (2015). Prediction with missing data via Bayesian additive regression trees. *The Canadian Journal of Statistics* 43(2), 224–239.
- Kent, D. M. and R. A. Hayward (2007). Limitations of applying summary results of clinical trials to individual patients - The need for risk stratification. *Journal of the American Medical Association* 298(10), 1209 – 1212.
- Kuo, L. and B. Mallick (1997). Bayesian semiparametric inference for the accelerated failure-time model. *The Canadian Journal of Statistics* 25(4), 457–472.
- Lamont, A., M. D. Lyons, T. Jaki, E. Stuart, D. J. Feaster, K. Tharmaratnam, D. Oberski, H. Ishwaran, D. K. Wilson, and M. L. V. Horn (2016). Identification of predicted individual treatment effects in randomized clinical trials. *Statistical Methods in Medical Research - online version*.
- Lipkovich, I., A. Dmitrienko, and R. B. D’Agostino (2016). Tutorial in biostatistics: data-driven subgroup identification and analysis in clinical trials. *Statistics in Medicine* 36(1), 136–196.
- Loh, W.-Y., X. He, and M. Man (2015). A regression tree approach to identifying subgroups with differential treatment effects. *Statistics in Medicine* 34, 1818–1833.
- Louis, T. A. (1981). Nonparametric analysis of an accelerated failure time model. *Biometrika* 68(2), 381–390.



- Louis, T. A. and W. Shen (1999). Innovations in Bayes and empirical Bayes methods: estimating parameters, populations, and ranks. *Statistics in Medicine* 18, 2493–2505.
- Robins, J. and A. A. Tsiatis (1992). Semiparametric estimation of an accelerated failure time model with time-dependent covariates. *Biometrika* 79(2), 311–319.
- Shen, W. and T. A. Louis (1998). Triple-goal estimates in two-stage, hierarchical models. *Journal of Royal Statistical Society Series B* 60, 455–471.
- Shen, Y. and T. Cai (2016). Identifying predictive markers for personalized treatment selection. *Biometrics* 72, 1017–1025.
- Sparapani, R. A., B. R. Logan, R. E. McCulloch, and P. W. Laud (2016). Nonparametric survival analysis using Bayesian additive regression trees (BART). *Statistics in Medicine* 35, 2741–2753.
- Su, X., C.-L. Tsai, H. Wang, D. M. Nickerson, and B. Li (2009). Subgroup analysis via recursive partitioning. *Journal of Machine Learning Research* 10, 141–158.
- The SOLVD Investigators (1991). Effect of enalapril on survival in patients with reduced left ventricular ejection fraction and congestive heart failure. *The New England Journal of Medicine* 325(5), 293–302.
- Tian, L., A. A. Alizaden, A. J. Gentles, and R. Tibshirani (2014). A simple method for detecting interactions between a treatment and a large number of covariates. *Journal of the American Statistical Association* 109, 1517–1532.
- Tian, L., T. Cai, E. Goetghebeur, and L. Wei (2007). Model evaluation based on the sampling distribution of estimated absolute prediction error. *Biometrika* 94(2), 297–311.
- Tian, L., L. Zhao, and L. Wei (2014). Predicting the restricted mean event time with the subject’s baseline covariates in survival analysis. *Biostatistics* 15(2), 222–233.
- Tiwala, B., M. C. Jones, and D. J. Hand (2008). Good methods for coping with missing data in decision trees. *Pattern Recognition Letters* 29, 950–956.



- Wei, L. (1992). The accelerated failure time model: a useful alternative to the Cox regression model in survival analysis. *Statistics in Medicine* 11, 1871–1879.
- Weisberg, H. I. and V. P. Pontes (2015). Post hoc subgroups in clinical trials: Anathema or analytics? *Clinical Trials* 12(4), 357–364.
- Xu, Y., M. Yu, Y.-Q. Zhao, Q. Li, S. Wang, and J. Shao (2015). Regularized outcome weighted subgroup identification for differential treatment effects. *Biometrics* 71, 645–653.
- Yamato, H. (1984). Characteristic functions of means of distributions chosen from a Dirichlet process. *The Annals of Probability* 12(1), 262–267.
- Yang, M., D. B. Dunson, and D. Baird (2010). Semiparametric Bayes hierarchical models with mean and variance constraints. *Computational Statistics & Data Analysis* 54(9), 2172–2186.
- Zhao, Y., D. Zheng, A. J. Rush, and M. R. Kosorok (2012). Estimating individualized treatment rules using outcome weighted learning. *Journal of the American Statistical Association* 107(499), 1106–1118.
- Zhao, Y. Q., D. Zheng, E. B. Laber, R. Song, M. Yuan, and M. R. Kosorok (2015). Doubly robust learning for estimating individualized treatment with censored data. *Biometrika* 102(1), 151–168.